









Reproducibility of 3 T APT-CEST in Healthy Volunteers and Patients With Brain Glioma

Ivar J.H.G. Wameling, MSc,^{1*}  Joost P.A. Kuijer, PhD,² Beatriz E. Padrela, MSc,² 
 Yi Zhang, PhD,³  Frederik Barkhof, MD, PhD,^{2,4}  Henk J.M.M. Mutsaerts, MD, PhD,² 
 Jan Petr, PhD,^{1,5}  Elsmarieke van de Giessen, MD, PhD,^{1,2}  and Vera C. Keil, MD, PhD¹ 

Background: Amide proton transfer (APT) imaging is a chemical exchange saturation transfer (CEST) technique offering potential clinical applications such as diagnosis, characterization, and treatment planning and monitoring in glioma patients. While APT-CEST has demonstrated high potential, reproducibility remains underexplored.

Purpose: To investigate whether cerebral APT-CEST with clinically feasible scan time is reproducible in healthy tissue and glioma for clinical use at 3 T.

Study Type: Prospective, longitudinal.

Subjects: Twenty-one healthy volunteers (11 females; mean age \pm SD: 39 ± 11 years) and 6 glioma patients (3 females; 50 ± 17 years: 4 glioblastomas, 1 oligodendroglioma, 1 radiologically suspected low-grade glioma).

Field Strength/Sequence: 3 T, Turbo Spin Echo - amplifying perfection with application optimized contrasts using different flip angle evolution - chemical exchange saturation transfer (TSE SPACE-CEST).

Assessment: APT-CEST measurement reproducibility was assessed within-session (glioma patients, scan session 1; healthy volunteers scan sessions 1, 2, and 3), between-sessions (healthy volunteers scan sessions 1 and 2), and between-days (healthy volunteers, scan sessions 1 and 3). The mean APT_{CEST} values and standard deviation of the within-subject difference (SD_{diff}) were calculated in whole tumor enclosed by regions of interest (ROIs) in patients, and eight ROIs in healthy volunteers—whole-brain, cortical gray matter, putamen, thalami, orbitofrontal gyri, occipital lobes, central brain—and compared.

Statistical Tests: Brown-Forsythe tests and variance component analysis (VCA) were used to assess the reproducibility of ROIs for the three time intervals. Significance was set at $P < 0.003$ after Bonferroni correction.

Results: Intratumoral mean APT_{CEST} was significantly higher than APT_{CEST} in healthy-appearing tissue in patients ($0.5 \pm 0.46\%$). The average within-session, between-sessions, and between-days SD_{diff} of healthy control brains was 0.2% and did not differ significantly with each other ($0.76 > P > 0.22$). The within-session SD_{diff} of whole-brain was 0.2% in both healthy volunteers and patients, and 0.21% in the segmented tumor. VCA showed that within-session factors were the most important (60%) for scanning variance.

Data Conclusion: Cerebral APT-CEST imaging may show good scan-rescan reproducibility in healthy tissue and tumors with clinically feasible scan times at 3 T. Short-term measurement effects may be the dominant components for reproducibility.

Level of Evidence: 2

Technical Efficacy: Stage 2

J. MAGN. RESON. IMAGING 2022.

Novel imaging biomarkers in glioma patients may help improving tumor characterization and delineation.¹⁻³ One diagnosis, prognosis, and treatment decisions by such imaging biomarker is amide proton transfer (APT)

View this article online at wileyonlinelibrary.com. DOI: 10.1002/jmri.28239

Received Feb 23, 2022, Accepted for publication Apr 29, 2022.

*Address reprint requests to: I.J.H.G.W., De Boelelaan 1117, 1081 HV Amsterdam, The Netherlands. E-mail: ij.wameling@amsterdamumc.nl

Disclosures of Frederik Barkhof are: Steering committee or iDMC member for Biogen, Merck, Roche, Eisai and Prothena. Consultant for Roche, Biogen, Merck, IXICO, Jansen, Combinostics. Research agreements with Merck, Biogen, GE Healthcare, Roche. Co-founder and shareholder of Queen Square Analytics LTD.

From the ¹Department of Radiology and Nuclear Medicine, Cancer Center Amsterdam, Amsterdam University Medical Center, Amsterdam, The Netherlands;

²Department of Radiology and Nuclear Medicine, Amsterdam Neuroscience, Amsterdam University Medical Center, Amsterdam, The Netherlands; ³Key Laboratory for Biomedical Engineering of Ministry of Education, Department of Biomedical Engineering, College of Biomedical Engineering & Instrument Science, Zhejiang University, Hangzhou, China; ⁴Queen Square Institute of Neurology and Centre for Medical Image Computing, University College London, London, UK; and ⁵Helmholtz-Zentrum Dresden-Rossendorf, Institute of Radiopharmaceutical Cancer Research, Dresden, Germany

Additional supporting information may be found in the online version of this article

This is an open access article under the terms of the [Creative Commons Attribution-NonCommercial-NoDerivs](https://creativecommons.org/licenses/by-nc-nd/4.0/) License, which permits use and distribution in any medium, provided the original work is properly cited, the use is non-commercial and no modifications or adaptations are made.

imaging. APT is a subset of chemical exchange saturation transfer (CEST) imaging that allows for quantitative amide and peptide detection.^{1,4,5} Specifically, APT-CEST may be especially useful in glioma imaging as these primary brain tumors express increased amounts of protein.^{6–8} This magnetic resonance imaging (MRI) technique measures the intensity change in bulk water after the magnetization in amide protons is selectively saturated and transferred by chemical exchange to water protons.⁶ This intensity change indirectly reflects protein concentration in the tissue, computed by the magnetization transfer ratio asymmetry (MTR_{asym}).^{4,5,9}

Multiple clinical applications have been proposed in recent years for neuro-oncological APT-CEST imaging and show promising results regarding diagnosis, characterization, and treatment planning and monitoring in glioma.^{8,10–14} Also in other clinical contexts, APT-CEST has demonstrated its potential clinical usability, eg, in the detection of stroke for highlighting ischemic areas, paving its way to a near-future standard application.^{15–17} However, particularly for routine clinical application, high reproducibility in healthy and tumorous tissue is crucial. Quantitative assessment of the reproducibility of differences between healthy and tumorous tissue is mandatory for the development of imaging biomarkers with established cut-off values to non-invasively differentiate between tissue conditions.

Previous preliminary findings in reproducibility studies were promising for clinical 3 T APT-CEST applications.^{18–20} One study showed consistently higher within-session than between-sessions reproducibility for 3 T APT-CEST with partial brain coverage and relatively long scanning time in healthy volunteers and glioma patients.¹⁸ Another study found good reproducibility in brain tumors.¹⁹ Spatially homogenous radio-frequency (RF) shimming and B₀-inhomogeneity correction could contribute to this reproducibility, but the authors of this study exclusively investigated mean tumor APT-CEST values in a single slice. A third study found good reproducibility in only two healthy volunteers.²⁰

The purpose of this study was to investigate the short- and long-term reproducibility of 3 T APT-CEST measurements in a comparatively large group of healthy volunteers and a pilot level group of glioma patients, with a clinically applicable scan protocol with full brain coverage and a short scan duration.

Methods

This prospective study was approved by the institutional review board (VUmc_2021-0038) and written informed consent was obtained from all participants.

Study Design

Healthy volunteers were recruited non-commercially through external advertisements. Inclusion criteria were 1) age >18 years and 2) neither clinical history nor MRI evidence of brain pathology. Prospective recruitment also included

patients with suspected recurrent or de-novo glioma on external MRI and referred for tumor resection between May 2021 and July 2021. Patients were included if 1) age >18 years, 2) they had a radiological diagnosis of de-novo glioma or recurrent already confirmed glioma, 3) received clinically indicated MRI, and 4) had no other concurrent brain pathology at the time of diagnosis.

Participants with severe motion artifacts in T1-weighted (T1w), contrast-enhanced T1-weighted (ceT1w), or APT-CEST scans were excluded. No participants needed to be excluded due to compromised image quality.

Participants

Twenty-one healthy volunteers (mean age \pm SD: 39 \pm 11 years, 11 women) and 6 glioma patients (mean age \pm SD: 50 \pm 17 years, 3 women) were scanned. Five patients subsequently received a histopathological confirmation according to the 2021 World Health Organization (WHO) criteria: four glioblastomas (GBMs; WHO grade 4) and one oligodendroglioma (WHO grade 2).²¹ One patient opted against surgery due to the high radiological likelihood of a slow-growing low-grade glioma. Power analysis to determine group size to detect change in APT-CEST for GBM and LGG is given in Table S1 in the Supplemental Material.

Protocol of Scan–Rescan Test

Healthy volunteers were subjected to three APT-CEST scan sessions (Fig. 1). The first two sessions were separated by participant repositioning (between-sessions reproducibility) and the last session occurred 4–14 days later (between-days reproducibility). Patients underwent one scan session (Fig. 1). Each session, in both volunteers and patients, contained two consecutive APT-CEST scans (within-session reproducibility) with a B₀-map in between. All participants received a structural three-dimensional (3D) T1-weighted acquisition (T1w) while the patients additionally received a complete neuro-oncological MRI protocol according to the European Organisation for Research and Treatment of Cancer standard including 3D T1-weighted post-contrast (ceT1w) and fluid-attenuated inversion recovery.²² APT-CEST scanning was performed before the neuro-oncological MRI protocol.

APT-CEST Image Acquisition and Post-Processing

All participants were scanned on a 3-T MRI (Vida, Siemens Healthineers, Erlangen, Germany) using a 20-channel head coil, including whole-brain 3D MPRAGE T1w (repetition time (TR) 2300 msec, echo time (TE) 2.32 msec, inversion time (TI) 900 msec, refocusing flip angle 8°, field of view 240 mm, slice thickness 0.9 mm) and TSE SPACE APT-CEST (TR 3000 msec, TE 17 msec, turbo factor 140, refocusing flip angle 120°, 2.8 \times 2.8 \times 2.8 mm³ resolution, 7 frequencies with saturation pulses [10 Gaussian pulses of 100 msec at 2.0 μ T] at \pm 3.0 ppm, \pm 3.5 ppm, \pm 4.0 ppm,

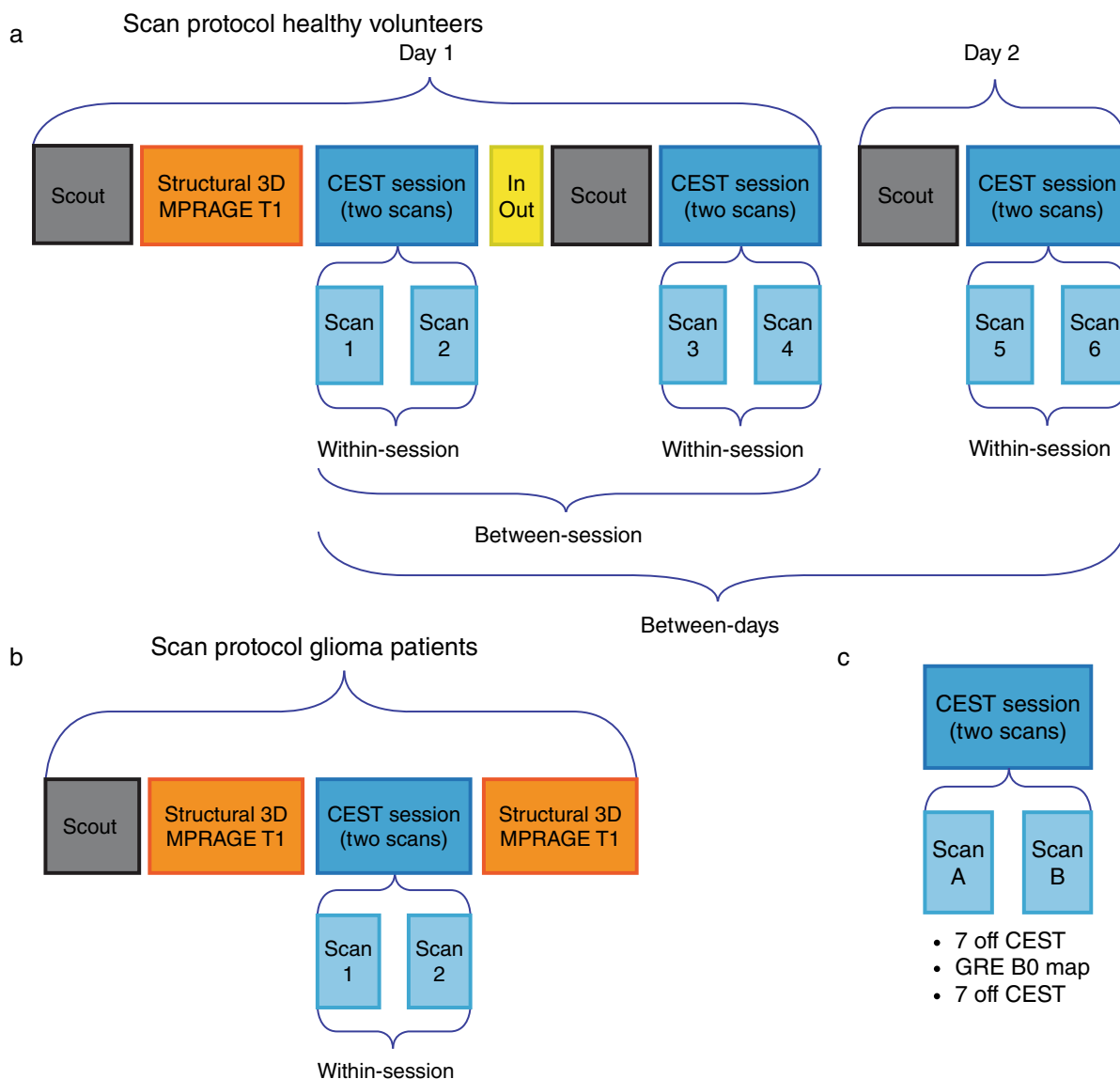


FIGURE 1: (a) Scan protocol for the healthy volunteers. (b) Scan protocol for the patients. (c) Scan session. A session contains two consecutive APT-CEST scans and one B0 map. (a) Scans: 1 = baseline, 2 = scan directly after the baseline—i.e., 1–2 = within-session reproducibility—scan 4 is a scan 30 minutes after the first—i.e., 1–4 = between-sessions reproducibility—scan 6 = another day—i.e., 1–6 = between-day reproducibility. (b) Glioma patients underwent one session.

and 1560 ppm off-resonance, scan duration: 4:36 minutes) plus a dual-echo gradient recalled echo (GRE) B0 map for correction of spatial inhomogeneity of the resonance frequency.²³

All off-resonance scans were registered to the 1560 ppm off-resonance scan to correct for head motion (MCFLIRT, FSL 5.0.9).²⁴ APT-CEST maps were then calculated as MTR_{asym} at 3.5 ppm off-resonance from motion-corrected images:

$$APT_{\text{CEST}} = \frac{MTR_{\text{asym}}(3.5 \text{ ppm})}{S_0} = \frac{S_{\text{sat}}(-3.5 \text{ ppm}) - S_{\text{sat}}(3.5 \text{ ppm})}{S_0}$$

The S_{sat} and S_0 represent the imaging signal intensities measured with RF saturation at ± 3.5 ppm and at

1560 ppm, respectively. The B0 map was expressed in ppm after unwrapping by FSL (Version 5.0.9) Prelude. The measured points on the Z-spectrum (off-resonance saturation spectrum) were interpolated to the actual frequency shift as measured by the B0 map. We extrapolated the measured points on the Z-spectrum if the frequency shift was between ± 0.5 ppm and ± 1 ppm. Voxels with a shift larger than 1 ppm were masked (set to 0). Next, the 1560 ppm off-resonance APT-CEST scan was registered to the non-contrast 3D T1w image with co-registration of the APT-CEST map using FLIRT (FSL 5.0.9) for healthy volunteers and patients.²⁴ The 3D T1w scan was spatially normalized to Montreal Neurosciences Institute (MNI) space using CAT12.7 (build 1615)²⁵ and again with co-registration of the APT-CEST map, which was then

smoothed by a $3.5 \times 3.5 \times 3.5 \text{ mm}^3$ full width at half maximum (FWHM) Gaussian filter. No skull stripping was performed.

Image Analysis

Five anatomical regions of interest (ROIs) were available in MNI space using the Harvard-Oxford atlas²⁶: the whole brain including cerebellum and internal cerebral spinal fluid spaces, cortical gray matter, deep white matter, putamen, and thalami. Three additional anatomical ROIs were manually delineated near the orbitofrontal gyri, the occipital lobes, and the central brain by (I.J.H.G. Wameling) with 1 year of experience under supervision of a neuroradiologist with 10 years of experience (V.C. Keil) (Fig. 2). The orbitofrontal gyri represent a region that is susceptible to B0-inhomogeneities.²⁷ All three ROIs contained both white and gray matter.

In patients with glioma, the ROIs enclosing presumably vital glioma tissue were manually delineated, together with similar-sized contralateral tissue ROIs, on the ceT1w for enhancing tumors and based on FLAIR for the non-enhancing tumors by a neuroradiologist with 10 years of experience (V.C. Keil).

By multiplying the binary ROI atlases with the APT-CEST scans the mean APT_{CEST} values were calculated for all scans. Next, the SD across all measurements was taken for the eight ROIs. The SD across subjects of the within-subject difference (SD_{diff}) between the mean APT_{CEST} values was calculated for the eight ROIs and each of the three reproducibility time intervals—within-session, between-sessions, and between-days. Additionally, voxel-wise SD_{diff} maps were computed from non-averaged APT_{CEST} values for the three

reproducibility time intervals to visually identify locations of low reproducibility.

Statistics

The Brown-Forsythe test (Python, Python Software Foundation, version 3.6.9, package: Scipy, version 1.5.2) was used to test the variance of the SD_{diff} among the three reproducibility time intervals of the eight anatomical ROIs. Bonferroni correction was performed by dividing the significance threshold (0.05) by the number of separate tests ($8 \text{ ROIs} \times 2 \text{ tests} = 16$). Variance component analysis (VCA) (Rstudio Version: 1.4.1106; VCA Version: 1.4.3) was performed on the mean APT_{CEST} value of the eight anatomical ROIs to find the contributions of the different effects. The Brown-Forsythe test and VCA were only performed on healthy volunteers.

The agreement of the APT_{CEST} values in tumor patients was assessed by the intraclass correlation coefficient (ICC) (Python, Python Software Foundation, version 3.6.9, package: Pingouin, version 0.3.12). The within-session ICC was computed for the tumor and contralateral ROI. The ICCs were calculated with a 95% confidence interval (CI) using an average random raters model, and given the following classifications: 0.00–0.39, poor; 0.40–0.59, fair; 0.60–0.74, good; and 0.75–1.00 excellent.²⁸

Bland–Altman plots were created to show differences between the three reproducibility time intervals in healthy volunteers. The Mann–Whitney U test (Python, Python Software Foundation, version 3.6.9, package: Scipy, version 1.5.2) was performed to compare the mean APT_{CEST} values of the different structures in healthy volunteers with the mean tumor values in patients. Statistical significance was determined at $P < 0.006$ with Bonferroni correction (0.05/8).

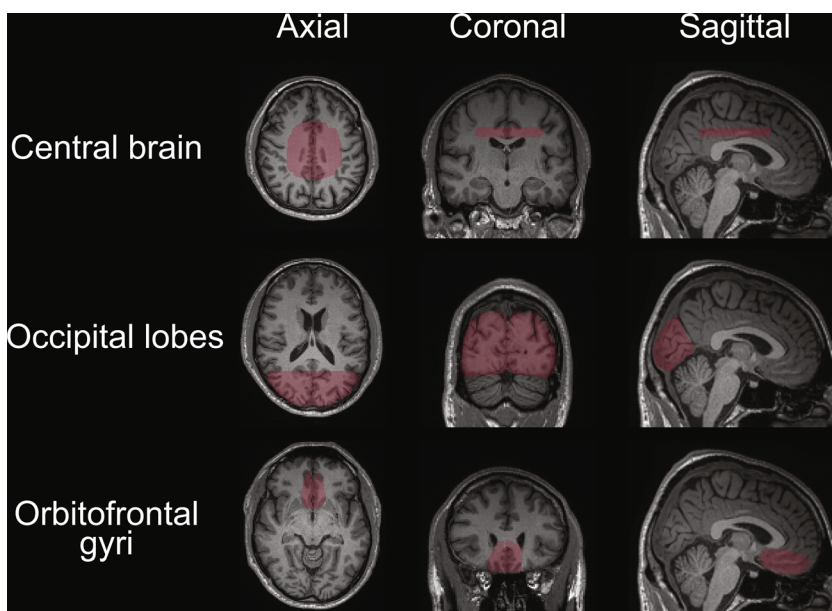


FIGURE 2: Axial, coronal, and sagittal slices of the three manually delineated regions of interest (ROIs).

The effect size (E) was only computed for patients:

$$\text{Effect size } (E) = \frac{\text{Tumor-to-normal tissue difference}}{\text{SD}_{\text{diff}}}$$

Results

APT_{CEST} Descriptive Statistics in Volunteers and Patients

The mean and SD for the anatomical and tumor ROIs are shown in Table 1. The mean APT_{CEST} difference between ROIs in GBMs and contralateral tissue was 1.11% ($N = 4$, Table 1, Fig. 3). Intratumoral mean APT_{CEST} ($1.59 \pm 0.67\%$, $N = 6$) was significantly higher than contralateral similar-sized ROI APT_{CEST} in healthy-appearing tissue in patients ($0.5 \pm 0.46\%$), and also significantly higher than mean APT_{CEST} in anatomical ROIs in healthy volunteers (between 0.42 and 1.02, $N = 21$).

Reproducibility in Healthy Volunteers

Figure 4 shows high within-session reproducibility and only slightly higher between-sessions and between-days voxel-wise SD_{diff} . The highest within-session voxel-wise SD_{diff} variance was found in the orbitofrontal gyri, as also shown by the higher ROI SD_{diff} (Table 2). The SD_{diff} was consistent within each of the three time intervals and only showed a small increase (maximum of 0.11%) between them.

The between-days SD_{diff} was consistently slightly lower than the between-sessions SD_{diff} . However, the Brown-Forsythe test showed a non-significant difference between the between-sessions and between-days reproducibility ($P = 0.75$, $N = 21$). The SD_{diff} increase between sessions was small and the reproducibility did not significantly differ between the within-session and between-sessions and the within-session and between-days (Table 2). No statistically significant differences were found after Bonferroni correction. The within-session SD_{diff} of the whole brain for all patients was 0.2% ($N = 6$).

The VCA showed that total variance (0.03–0.07) was relatively low compared to the difference between GBMs and contralateral tissue (1.11%). The variance appears to be predominated by the factor within-session rather than any other factor (Table 3). This is consistent with the SD_{diff} maps (Fig. 4). Figures 5 and 6 show Bland–Altman plots of the mean APT_{CEST} value against the APT_{CEST} value session differences of the brain ROIs.

Reproducibility in Patients

The within-session reproducibility of the tumors was slightly lower (SD_{diff} 0.21%, $N = 6$) than in the contralateral ROIs (SD_{diff} 0.11%), but without a statistical significance ($P = 0.73$). The mean whole-brain APT_{CEST} values did not

Table 1. Mean Regional APT_{CEST} Values in Healthy Volunteers and Glioma Patients

| Dataset | Whole Brain | Cortical Gray Matter | Deep White Matter | Putamen | Thalami | Orbitofrontal Gyri | Occipital Lobes | Central Brain | Tumor ROI | Contralateral ROI |
|---------------------------------------|-----------------|----------------------|-------------------|-----------------|-----------------|--------------------|-----------------|-----------------|-----------------|-------------------|
| Healthy volunteers ($N = 21$) | 0.88 ± 0.93 | 0.82 ± 0.85 | 0.42 ± 0.53 | 0.95 ± 0.45 | 1.39 ± 0.46 | 0.26 ± 1.81 | 1.02 ± 0.65 | 0.87 ± 0.54 | | |
| Patients ($N = 6$) | 0.93 ± 0.95 | | | | | | | | 1.59 ± 0.67 | 0.5 ± 0.46 |
| GBM, WHO 4 ($N = 4$) | 1.02 ± 0.17 | | | | | | | | 1.93 ± 0.51 | 0.83 ± 0.34 |
| Oligodendroglioma, WHO 2 ($N = 1$) | 0.66 ± 0.04 | | | | | | | | 0.57 ± 0.29 | 0.14 ± 0.05 |
| LGG, radiologically WHO 2 ($N = 1$) | 0.93 ± 0.06 | | | | | | | | 1.24 ± 0.04 | 0.14 ± 0.02 |

APT_{CEST} = amide proton transfer chemical exchange saturation transfer; GBM = glioblastoma; LGG = low grade glioma; ROI = region of interest.

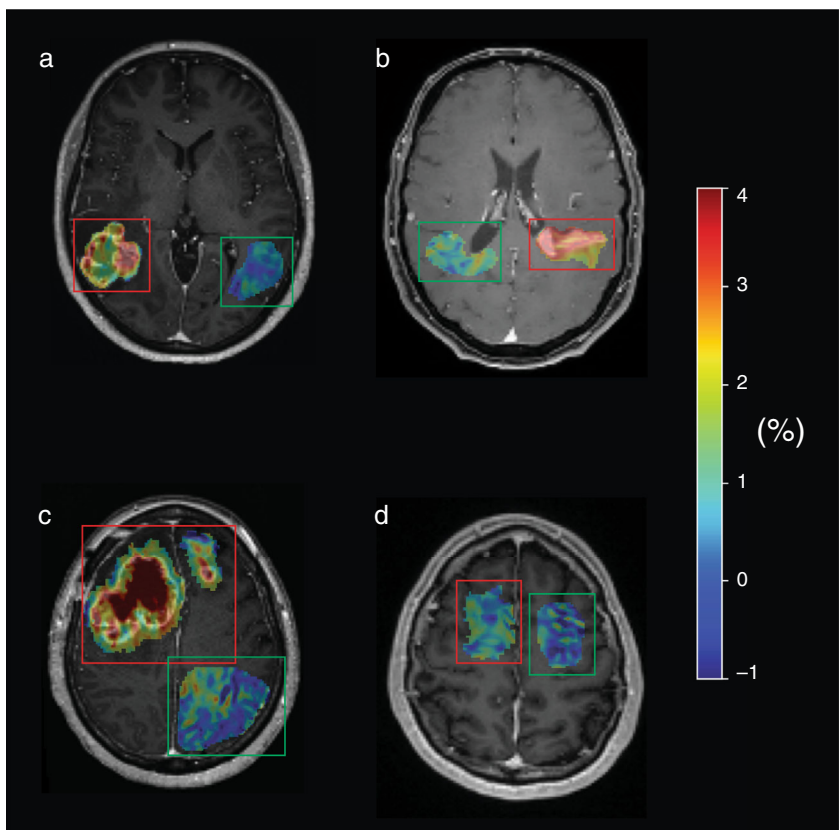


FIGURE 3: Single transversal APT-CEST slices of four different glioblastoma patients. APT_{CEST} value in color scale projected on the post-contrast T1-weighted image, within the tumor ROI only. Red and green boxes are positioned around the tumor and contralateral ROIs, respectively. Note the heterogeneous hyperintensity in the tumorous regions that show hyperintensity on the contrast-enhanced T1-weighted image when compared to the contralateral region (a–c). (d) The APT-CEST value of a non-enhancing glioblastoma. APT = amide proton transfer; CEST = chemical exchange saturation transfer; ROI = region of interest.

significantly differ between healthy volunteers and patients ($0.88 \pm 0.93\%$, $0.93 \pm 0.95\%$ respectively; $P = 0.13$). Mean tumor values did however differ significantly with the eight ROIs in healthy volunteers. Within-session scan agreement was the highest in contralateral ROIs (ICC = 0.99; 95% CI, 0.92–1.00; $N = 21$) followed by glioma (ICC = 0.97; 95% CI, 0.82–1.00; $N = 6$). The effect size of

the APT_{CEST} in GBM was 5 when considering the ROI-wise within-session SD_{diff} of the putamen.

Discussion

We found high reproducibility across the three reproducibility time intervals in healthy volunteers. Within-session

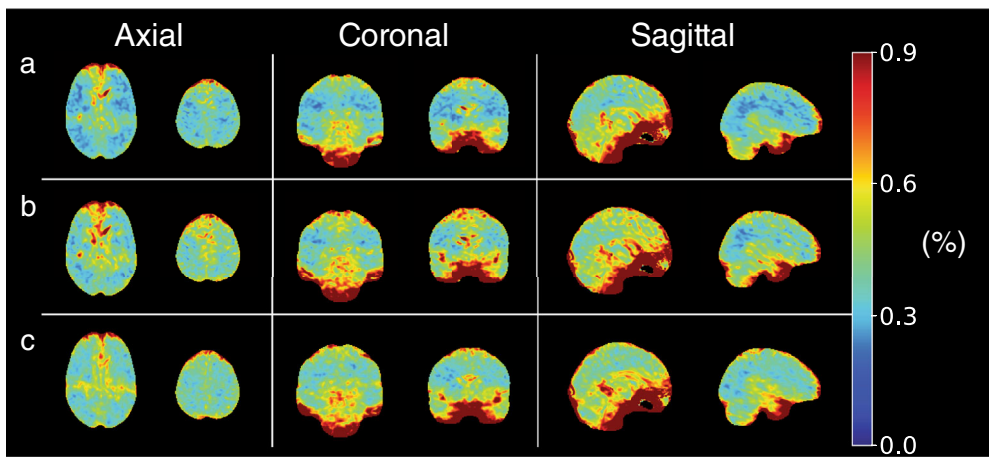


FIGURE 4: Voxel-wise SD maps of the within-subject difference between scan sessions 1–2, 1–4, and 1–6 (rows a, b, and c, respectively), for all healthy volunteers ($N = 21$). Color scale represents the SD of the difference in APT_{CEST} value (%) between sessions (SD_{diff}), where higher SD_{diff} means lower reproducibility.

Table 2. The SD_{diff} of the Eight ROIs and Each of the Three Reproducibility Time Intervals

| | Whole Brain | Cortical Gray Matter | Deep White Matter | Putamen | Thalami | Orbitofrontal Gyri | Occipital Lobes | Central Brain |
|----------------------|-------------|----------------------|-------------------|------------|------------|--------------------|-----------------|---------------|
| Within-session (%) | 0.20 | 0.20 | 0.19 | 0.22 | 0.26 | 0.61 | 0.22 | 0.20 |
| Between-sessions (%) | 0.24 | 0.25 | 0.26 | 0.28 | 0.28 | 0.67 | 0.26 | 0.27 |
| | $P = 0.35$ | $P = 0.28$ | $P = 0.39$ | $P = 0.22$ | $P = 0.31$ | $P = 0.76$ | $P = 0.33$ | $P = 0.33$ |
| Between-days (%) | 0.22 | 0.22 | 0.24 | 0.33 | 0.33 | 0.48 | 0.24 | 0.26 |
| | $P = 0.17$ | $P = 0.20$ | $P = 0.11$ | $P = 0.01$ | $P = 0.05$ | $P = 0.58$ | $P = 0.14$ | $P = 0.03$ |

The P -value is the comparison between the within-session difference and either the between-sessions and or between-days difference for the brain structures in healthy volunteers. P -values less than 0.003 were considered significant.

SD_{diff} = standard deviation across subjects of the within-subject difference; ROI = region of interest.

measurement agreement in glioma, contralateral-to-glioma, and healthy brain ROIs was excellent. Furthermore, within-session reproducibility in whole-brain APT-CEST scans of glioma patients was equal to the reproducibility in healthy volunteers and even better for tumor ROIs. The variance thus seems to be predominated by general error contributors such as thermal noise, subject motion, B0 inhomogeneity, and stress on scanner hardware, rather than long-term instrumental errors, physiological variance, or between-subject differences. These results may suggest that 3 T APT-CEST provides sufficient reproducibility for clinical application, especially given the larger APT_{CEST} value changes between glioma and normally appearing tissue.

While the between-sessions reproducibility was not evaluated previously, the within-session and between-days reproducibility of APT-CEST scans of this study are in line with previous studies in healthy volunteers^{18,20} and brain tumor patients.^{18–20} The within-session, between-sessions, and between-days reproducibility presented in the current study showed a trend of decrease—although not statistically

significant—for the SD_{diff} and the VCA. Between-days reproducibility showed higher consistency than between-sessions reproducibility, albeit not to a statistically significant degree. The first two studies used scan protocols and acquisition parameters similar to ours with an exclusive focus on mean APT_{CEST} values.^{18,19} Our current study pursues a different perspective by also performing a voxel-wise reproducibility analysis in healthy tissue of patients and healthy participants to focus on the reproducibility of relative APT_{CEST} values. Both studies found similar within-session scan agreement for glioma.^{18,19}

Our results show that the different imaging sessions had no statistically significant effect on APT_{CEST} measurement values, which is in agreement with a previous similar analysis of variance in healthy volunteers and glioma patients.¹⁸ Our findings are comparable to another study with two healthy volunteers.²⁰ Furthermore, our difference between glioma measurements and healthy appearing contralateral tissue at all time points was in agreement with previous studies.^{13,18,29} While APT-CEST reproducibility in the brain has not yet

Table 3. Percentage of Total Variance Computed by the Variance Component Analysis

| | Whole Brain | Cortical Gray Matter | Deep White Matter | Putamen | Thalami | Orbitofrontal Gyri | Occipital Lobes | Central Brain |
|--|-------------|----------------------|-------------------|------------|------------|--------------------|-----------------|---------------|
| Total variance (APT _{CEST} %) | 0.033 | 0.039 | 0.034 | 0.069 | 0.058 | 0.205 | 0.041 | 0.043 |
| Factor subject | 16% | 28% | 11% | 34% | 13% | 42% | 12% | 22% |
| Factor day | 19% | 16% | 21% | 16% | 4% | 14% | 20% | 8% |
| Factor session | 5% | 2% | 13% | 14% | 22% | 1% | 8% | 24% |
| Factor within-session | 60% | 54% | 55% | 36% | 61% | 43% | 60% | 46% |

Largest contributor to total variance is marked in bold.

APT_{CEST} = amide proton transfer chemical exchange saturation transfer.

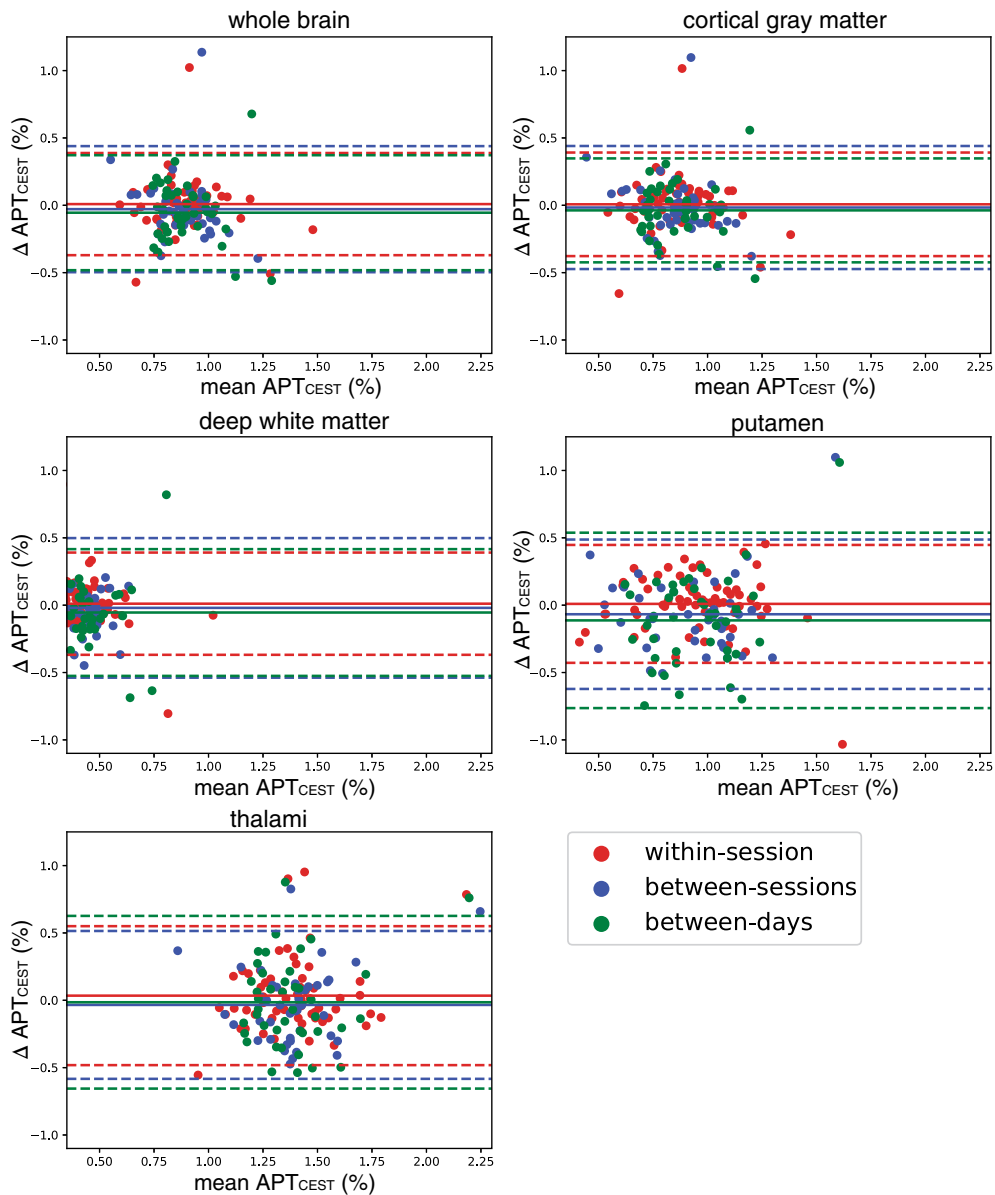


FIGURE 5: Bland–Altman plots. Amide proton transfer chemical exchange saturation transfer (APT_{CEST}) differences of the five different brain structures are plotted against their mean APT_{CEST} value. Continuous and broken lines indicate mean difference and 95% limits of agreement (mean difference \pm 1.96 SD of the paired difference) respectively.

been investigated extensively, our reproducibility was similar to that of studies in other body parts such as breast (7 T) and prostate (3 T) tissue and different CEST sequences such as glutamate-CEST.^{30–33}

We found the lowest reproducibility in the orbitofrontal gyri, which can be explained by the susceptibility of these regions to B0-inhomogeneity that impacts the Z-spectrum.¹³ Moreover, regions with large veins, such as areas close to the superior sagittal sinus, also showed high variance consistent with the literature.²⁹ We corrected for the B0-inhomogeneity by creating a B0-map between both APT-CEST scans.³⁴ The B0-map was scanned once for each session in order to limit the session duration. We thus implicitly assumed that the measurement error of the B0-map itself does not contribute

to APT_{CEST} variability. However, the within-session variability does include subject motion between CEST and B0 scans. Other potential causes are subject movement in general, and the pre- and post-processing steps, which is why we applied the same sequence parameters during the entire study. Finally, low reproducibility could be caused by physiological variation of amide concentrations.

With good reproducibility, APT-CEST imaging shows potential for clinical implementation. The SD_{diff} was consistent within each of the three time intervals and only slightly increased between the different time intervals. Moreover, the SD_{diff} was small compared to the tumor signal change, denoting a detectable difference between healthy and tumorous tissue, in particular for GBMs. This opens the door for

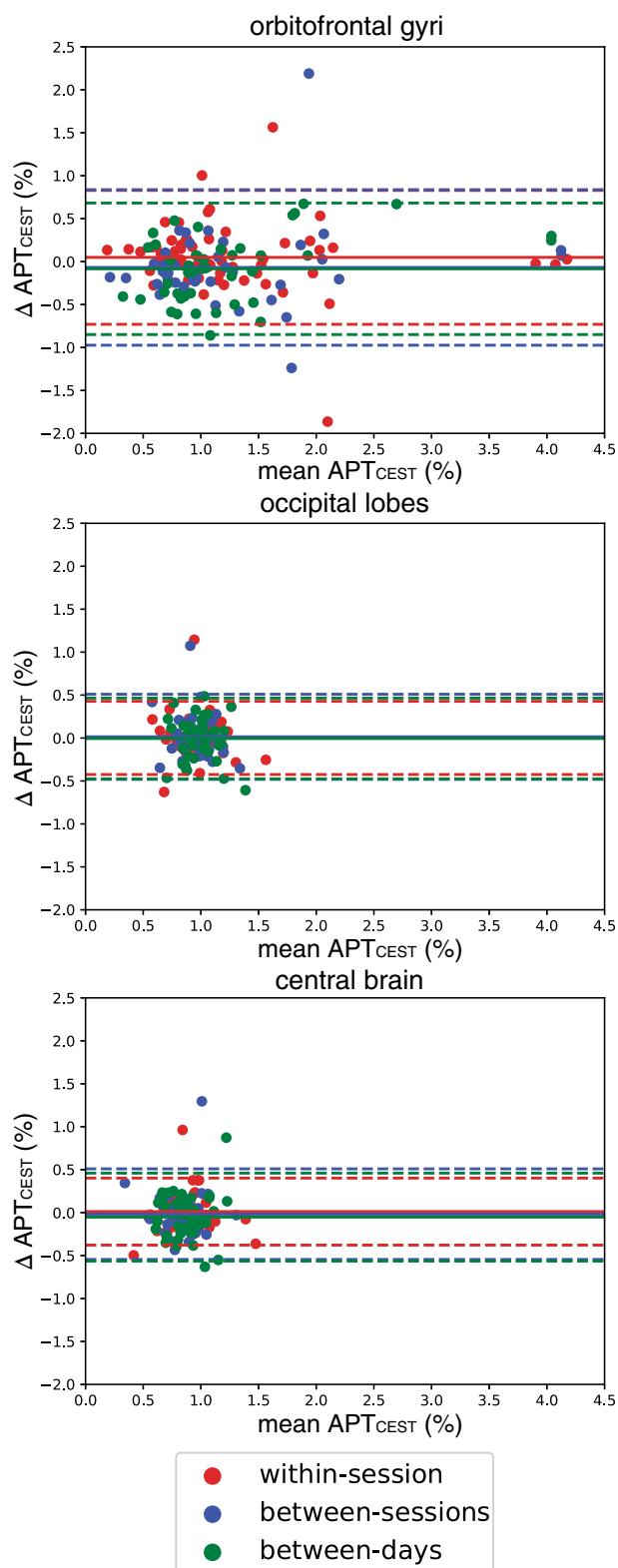


FIGURE 6: Bland-Altman plots. Showing differences of reproducibility in the orbitofrontal gyri, central brain, and occipital lobes. Note the larger limits of agreement in the orbitofrontal gyri and the narrower limits of agreement in the occipital lobes and central brain regions.

potential clinical biomarker applications such as percentage differences in APT-CEST values that can be used to differentiate tumors from viable tissue. A potential benefit of APT-

CEST over conventional tumor imaging, more specifically ceT1w imaging, is that APT-CEST might be able to identify non-contrast-enhancing parts of high-grade gliomas.²⁹ Previous studies have also shown that APT imaging is able to differentiate between solitary brain metastases and GBMs or radiation necrosis and viable tumor tissue.^{35–37} These findings are particularly important for quick and non-invasive disease staging and tumor classification, which may avoid unnecessary biopsies, but also open potential alternatives to gadolinium contrast administration.³⁸

Limitations

We only investigated at intra-vendor reproducibility in this study. It is thus unclear whether the results can be generalized to different scanners and vendors. Inter-vendor reproducibility is important to study for clinical implementation as scanning a patient on the same scanner for follow-up assessment is not always clinically feasible. Another limitation is that our sample size for glioma patients remains on a pilot study level. Finally, we could have scanned more offset frequencies to improve correction for off-resonance effects but this would have prolonged the scan duration to clinically unfeasible times.

Conclusion

The findings of this study indicate that whole-brain APT-CEST imaging with clinical scan time has a sufficiently high short- and long-term reproducibility in tumors and healthy tissue at clinically feasible scan times at 3 T. The tumor-normal tissue contrast was larger than the APT-CEST scan-rescan errors. Instrumental noise seems to be the largest component, while long-term physiological variance and between-subject variability were smaller. Reproducibility might be lower near regions with B0-inhomogeneity.

Acknowledgments

The authors thank T. Schweigmann for organizing the scanning of the patients. FB is supported by the NIHR Biomedical Research Center at UCLH. HM is supported by the Dutch Heart Foundation (03-004-2020-T049). The authors thank the COST Action CA 18206 Glimr 2.0 for their networking support.

References

- Booth TC, Williams M, Luis A, Cardoso J, Ashkan K, Shuaib H. Machine learning and glioma imaging biomarkers. *Clin Radiol* 2020;75:20-32.
- Henriksen OM, Del Mar Álvarez-Torres M, Figueiredo P, et al. High-grade glioma treatment response monitoring biomarkers: A position statement on the evidence supporting the use of advanced MRI techniques in the clinic, and the latest bench-to-bedside developments. Part 1: Perfusion and diffusion techniques. *Front Oncol* 2022;12: 810263.

3. Booth TC, Wieggers EC, Wamert EAH, et al. High-grade glioma treatment response monitoring biomarkers: A position statement on the evidence supporting the use of advanced MRI techniques in the clinic, and the latest bench-to-bedside developments. Part 2: Spectroscopy, chemical exchange saturation, multiparametric imaging, and Radiomics. *Front Oncol* 2021;11:811425.
4. Zhou J, Lal B, Wilson DA, Larterra J, van Zijl PCM. Amide proton transfer (APT) contrast for imaging of brain tumors. *Magn Reson Med* 2003;50:1120-1126.
5. Zhou J, Payen J-F, Wilson DA, Traystman RJ, van Zijl PCM. Using the amide proton signals of intracellular proteins and peptides to detect pH effects in MRI. *Nat Med* 2003;9:1085-1090.
6. Schmidt H, Schwenzer NF, Gatidis S, et al. Systematic evaluation of amide proton chemical exchange saturation transfer at 3 T: Effects of protein concentration, pH, and acquisition parameters. *Invest Radiol* 2016;51:635-646.
7. Scheidegger R, Wong ET, Alsop DC. Contributors to contrast between glioma and brain tissue in chemical exchange saturation transfer sensitive imaging at 3 Tesla. *Neuroimage* 2014;99:256-268.
8. Wen Z, Hu S, Huang F, et al. MR imaging of high-grade brain tumors using endogenous protein and peptide-based contrast. *Neuroimage* 2010;51:616-622.
9. van Zijl PCM, Yadav NN. Chemical exchange saturation transfer (CEST): What is in a name and what isn't? *Magn Reson Med* 2011;65:927-948.
10. Zou T, Yu H, Jiang C, et al. Differentiating the histologic grades of gliomas preoperatively using amide proton transfer-weighted (APT_w) and intravoxel incoherent motion MRI. *NMR Biomed* 2017;31:1-12.
11. Jiang S, Eberhart CG, Zhang Y, et al. Amide proton transfer-weighted magnetic resonance image-guided stereotactic biopsy in patients with newly diagnosed gliomas. *Eur J Cancer* 2017;83:9-18.
12. Dou W, Lin C-YE, Ding H, et al. Chemical exchange saturation transfer magnetic resonance imaging and its main and potential applications in pre-clinical and clinical studies. *Quant Imaging Med Surg* 2019;9:1747-1766.
13. Jones CK, Schlosser MJ, van Zijl PCM, Pomper MG, Golay X, Zhou J. Amide proton transfer imaging of human brain tumors at 3T. *Magn Reson Med* 2006;56:585-592.
14. Zhou J, Blakeley JO, Hua J, et al. Practical data acquisition method for human brain tumor amide proton transfer (APT) imaging. *Magn Reson Med* 2008;60:842-849.
15. Sun PZ. Consistent depiction of the acidic ischemic lesion with APT MRI-dual RF power evaluation of pH-sensitive image in acute stroke. *Magn Reson Med* 2021;87:850-858.
16. Foo LS, Harston G, Mehndiratta A, et al. Clinical translation of amide proton transfer (APT) MRI for ischemic stroke: A systematic review (2003-2020). *Quant Imaging Med Surg* 2021;11:3797-3811.
17. Foo LS, Larkin JR, Sutherland BA, et al. Study of common quantification methods of amide proton transfer magnetic resonance imaging for ischemic stroke detection. *Magn Reson Med* 2021;85:2188-2200.
18. Lee JB, Park JE, Jung SC, et al. Repeatability of amide proton transfer-weighted signals in the brain according to clinical condition and anatomical location. *Eur Radiol* 2020;30:346-356.
19. Togao O, Hiwatashi A, Keupp J, et al. Scan-rescan reproducibility of parallel transmission based amide proton transfer imaging of brain tumors. *J Magn Reson Imaging* 2015;42:1346-1353.
20. Goerke S, Breitling J, Korzowski A, et al. Clinical routine acquisition protocol for 3D relaxation-compensated APT and rNOE CEST-MRI of the human brain at 3T. *Magn Reson Med* 2021;86:393-404.
21. Louis DN, Perry A, Wesseling P, et al. The 2021 WHO classification of tumors of the central nervous system: A summary. *Neuro Oncol* 2021;23:1231-1251.
22. Ellingson BM, Bendszus M, Boxerman J, et al. Consensus recommendations for a standardized brain tumor imaging protocol in clinical trials. *Neuro Oncol* 2015;17:1188-1198.
23. Zhang Y, Yong X, Liu R, et al. Whole-brain chemical exchange saturation transfer imaging with optimized turbo spin echo readout. *Magn Reson Med* 2020;84:1161-1172.
24. Jenkinson M, Bannister P, Brady M, Smith S. Improved optimization for the robust and accurate linear registration and motion correction of brain images. *Neuroimage* 2002;17:825-841.
25. Gaser C, Dahnke R. CAT-A computational anatomy toolbox for the analysis of structural MRI data. 2016.
26. Makris N, Goldstein JM, Kennedy D, et al. Decreased volume of left and total anterior insular lobule in schizophrenia. *Schizophr Res* 2006;83:155-171.
27. Yoo S, Song H, Kim S-G, Shim WM, Lee S-K. Feasibility of head-tilted brain scan to reduce susceptibility-induced signal loss in the prefrontal cortex in gradient echo-based imaging. *Neuroimage* 2020;223:117265.
28. Hallgren KA. Computing inter-rater reliability for observational data: An overview and tutorial. *Tutor Quant Methods Psychol* 2012;8:23-34.
29. Zhou J, Zhu H, Lim M, et al. Three-dimensional amide proton transfer MR imaging of gliomas: Initial experience and comparison with gadolinium enhancement. *J Magn Reson Imaging* 2013;38:1119-1128.
30. Dula AN, Dewey BE, Arlinghaus LR, et al. Optimization of 7-T chemical exchange saturation transfer parameters for validation of glycosaminoglycan and amide proton transfer of fibroglandular breast tissue. *Radiology* 2015;275:255-261.
31. Evans VS, Torrealdea F, Rega M, et al. Optimization and repeatability of multipool chemical exchange saturation transfer MRI of the prostate at 3.0 T. *J Magn Reson Imaging* 2019;50:1238-1250.
32. Nanga RPR, DeBrosse C, Kumar D, et al. Reproducibility of 2D GluCEST in healthy human volunteers at 7 T. *Magn Reson Med* 2018;80:2033-2039.
33. Bagga P, Pickup S, Crescenzi R, et al. In vivo GluCEST MRI: Reproducibility, background contribution and source of glutamate changes in the MPTP model of Parkinson's disease. *Sci Rep* 2018;8:2883.
34. Schuenke P, Windschuh J, Roeloffs V, Ladd ME, Bachert P, Zaiss M. Simultaneous mapping of water shift and B1 (WASABI)—Application to field-inhomogeneity correction of CEST MRI data. *Magn Reson Med* 2017;77:571-580.
35. Yu H, Lou H, Zou T, et al. Applying protein-based amide proton transfer MR imaging to distinguish solitary brain metastases from glioblastoma. *Eur Radiol* 2017;27:4516-4524.
36. Mehrabian H, Desmond KL, Soliman H, Sahgal A, Stanisiz GJ. Differentiation between radiation necrosis and tumor progression using chemical exchange saturation transfer. *Clin Cancer Res* 2017;23:3667-3675.
37. Zhou J, Tryggstad E, Wen Z, et al. Differentiation between glioma and radiation necrosis using molecular magnetic resonance imaging of endogenous proteins and peptides. *Nat Med* 2011;17:130-134.
38. Falk Delgado A, Van Westen D, Nilsson M, et al. Diagnostic value of alternative techniques to gadolinium-based contrast agents in MR neuroimaging—a comprehensive overview. *Insights Imaging* 2019;10:84.